PRE-PRINT

Performance investigation of an ejector-assisted transcritical CO_2 heat pump with brazed plate tri-partite gas cooler for space heating and hot water production

Tom EBEL[(a)], Alireza ZENDEHBOUDI [(a)], Armin HAFNER [(a)], Dani C. SANCHEZ [(b)]

[(a)] Department of Energy and Process Engineering, Norwegian University of Science and Technology (NTNU), Kolbjørn Hejes v 1B, 7491 Trondheim, Norway, armin.hafner@ntnu.no

[(b)] SPF Institute for Solar Technology, OST Eastern Switzerland University of Applied Sciences, CH-8640, Rapperswil, Switzerland

ABSTRACT

The carbon dioxide (CO_2) heat pump water heater is recognized as a potential technology for the production of domestic hot water (DHW) and space heating (SH). In this paper, the performance of a transcritical CO_2 heat pump water heater with a tri-partite gas cooler is discussed using a numerical model. The heat pump operates in three modes: (1) DHW mode, (2) SH mode, and (3) DHW+SH mode, which provides space heating at 35 °C and hot water up to 70 °C. The simulation model is validated with the experimental data. The effects of different parameters on system performance are investigated, and the coefficient of performance (COP) of the system under different operating conditions is evaluated. The results show that higher heat sink outlet temperatures lower the COP and increase SH/DHW-Ratio for the investigated cases. The maximum COP is investigated for various heat loads by continuous high-pressure (HP) modulation, reaching highest values at 50 % to 60 % of maximum heat load. The SH/DHW-Ratio is investigated for the presented simulation cases in DHW+SH mode, reaching 0.68 to 1.06 for different heat loads.

Keywords: Transcritical CO_2 Heat Pump, Energy analysis, SH/DHW-Ratio, Tri-partite gas cooler.

1. INTRODUCTION

It is estimated that 30% of end-energy is used in buildings, of which the largest share is heat, used for space heating (SH) and domestic hot water (DHW) supply [1]. While SH energy expenditure will fall in the future, considering building modernization measures, DHW demand is expected stay on the same levels as today [2]. It is therefore vital to implement technologies, capable of supplying heat energy at DHW temperature levels with less environmental impact. As lifetimes of current heating devices approach their end and efficiency standards rise, heat pumps that utilize renewable energy can fill the emerging gap. With the spread of this technology, remaining environmental concerns must also be addressed. Synthetical refrigerants, adversely impacting the atmosphere, have to be substituted by naturally occurring substances. Transcritical heat pumps using CO_2 are known to reliably address environmental concerns. The advantageous heat rejection characteristics of transcritical CO_2 heat pumps have been studied numerically and experimentally in recent years [3–6]. In the supercritical state heat is rejected by cooling the single-phase supercritical fluid. Rather than by condensation, the sensible cooling leads to a larger difference between inlet- and outlet temperatures. This is especially beneficial for heating applications that need a large temperature raise e.g., the production of domestic hot water. Using the design of a tri-partite gas-cooler (GC) was shown to provide high efficiency by utilizing multiple heat sinks to advantageously match the heat rejection characteristics of CO_2 [7]. While the first prototype used helical tube-in-tube gas coolers, current research investigates a novel configuration with brazed plate heat exchangers [8]. To investigate this heat pump design, this study will utilize experimental test data to validate a numerical model, which intern is used to expand on new simulation cases. Subsequently, the performance of the heat pump will be further evaluated by investigating the effects of different parameters in the system COP and SH/DHW-Ratio.

2. METHODS

2.1. System Layout

The investigated transcritical CO_2 heat pump consists of an evaporator, a compressor, a tri-partite gas cooler, an internal heat exchanger (IHX), an ejector, a throttling valve, and a liquid separator. The system is shown in Figure 1.

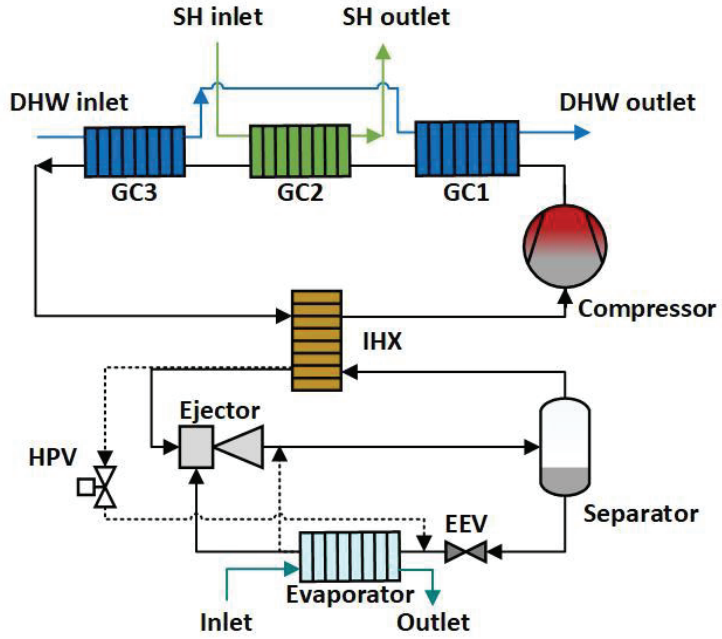

Figure 1: P&ID structure of the modelled CO_2 heat pump.

The pressure of evaporated refrigerant is raised in the ejector, after which the accumulator separates liquid from gaseous refrigerant. While the liquid CO_2 is returned back to the evaporator, the gaseous CO_2 continuous through the IHX and gets superheated. After the compressor raised the pressure from an intermediate to a high-pressure level, the refrigerant enters the three gas coolers. The gas coolers are used for reheating of DHW, SH, and preheating of the DHW in GC1, GC2 and GC3, respectively. The heat pump is designed for a heat duty of 10 kW in DHW and Parallel heating mode, while the maximum SH heat duty amounts up to 8 kW. The transcritical CO_2 rejects heat in the gas coolers before entering the HP side of the internal heat exchanger. Residual heat is utilized in IHX, to further cool down the refrigerant before it is throttled in the ejector.

2.2. Model Description and Control Strategy

A model of the CO_2 heat pump is developed to investigate the performance of the proposed unit. The basis is the object-oriented programming language Modelica [9], which is used in the Dymola 2021 modeling environment [10]. Furthermore, the component models are based on the TIL-library 3.9 from TLK-Thermo GmbH, with the TIL-Media-library 3.9 providing the fluid properties for CO_2 and water [11]. The model components are displayed in **Feil! Fant ikke referansekilden.**. All water side heat transfer coefficients are calculated using the single phase heat transfer coefficient (HTC) correlations by the Association of German Engineers [12]. The boiling HTC of the CO_2 is calculated using the correlations of Shah and Chen [13]. As the experimental pressure drops in the gas coolers amount to less than 0.5 % of the working pressure [14], its influence has been neglected during the simulations.

In order to reliably reach steady-state simulations, five PI-controllers are utilized in different parts of the cycle. The mass flow rates of the heat source water loop and the two heat sink water loops are adjusted by their respective controllers. Inlet and outlet temperatures get measured and the mass flow rate is adjusted to reach the desired temperature difference.

Table 1: Characteristics of the modelled components.

Component	Characteristic
Compressor	Type: Hermetic Twin Rotary
	Rated Rotational Speed: 6000 RPM
	Rated Displacement: 10 cm^3
Evaporator	Type: Brazed Plate Heat Exchanger
	Flow type: Counter Flow
	Plates: 40
	Plate Width: 0.111 m
	Plate length: 0.466 m
Internal Heat Exchanger	Type: Tube-in-Tube (Stainless Steel)
	Flow type: Counter Flow
	Area: 0.04 m^2
	Heat Transfer Coefficient: 2,000 $W/(m^2 \cdot K)$
Gas Coolers	Type: Brazed Plate Heat Exchanger (Stainless Steel)
	Flow type: Counter Flow
	Plates (GC1, GC2, GC3): 34, 80, 14
	Plate Width: 0.076 m
	Plate length: 0.154 m
Accumulator	Volume: 3 l
Ejector	Efficiency: 20 %

Switching of heating mode is achieved by setting the water mass flow rate in the DHW or SH boundary to $1 \cdot 10^{-4}$ kg/s, effectively shutting down heat transfer to the respective heat sink. The control of the throttling area of the expansion valve before the evaporator ensures to reach a set evaporation vapor quality, which was fixed at 0.85 for all simulations. The HP control gets exercised by the ejector. By comparing a set pressure level in the ejector PI-controller to the value in a pressure sensor, the nozzle area gets adjusted to reach the set HP value. The opening degree is varied by continuous modulation. Lastly, the compressor controller is used to provide a set amount of heating capacity. Once the required heating capacity is set, the compressor frequency gets adjusted to match heat outputs in the gas coolers. The controller can also be shut off, to manually set distinct compressor speeds. This enables to emphasize general trends in correlation to the frequency or the mass flow.

3. RESULTS AND DISCUSSION

The source data for all the presented results can be accessed via the link shown at the end of the refence list.

3.1. Model Validation

New correlations developed by Zendehboudi et al. [14] for the calculation of the supercritical HTC are implemented in the gas coolers. To validate the developed heat pump model, 25 test points from an experimental prototype are chosen to be compared to the model results. **Feil! Fant ikke referansekilden.** presents the deviation of the COP from the experimental results. The model predicts the COP within a deviation of 20 %. The absolute mean relative errors between the numerical and experimental COP values amount to 7.14 %, 5.79 % and 6.02 % for DHW, SH and Parallel mode, respectively. There are two factors that explain the existing differences in COP. First, the used model is a simplified version of the actual experimental setup. Second, it is observed that during the experiments heat is lost due to insufficient component insulation. Since the Modelica model represents an ideal model, it does not account for energy losses to the ambient. Overall, the deviation is still within the expected range and the model will therefore be used for new simulation cases.

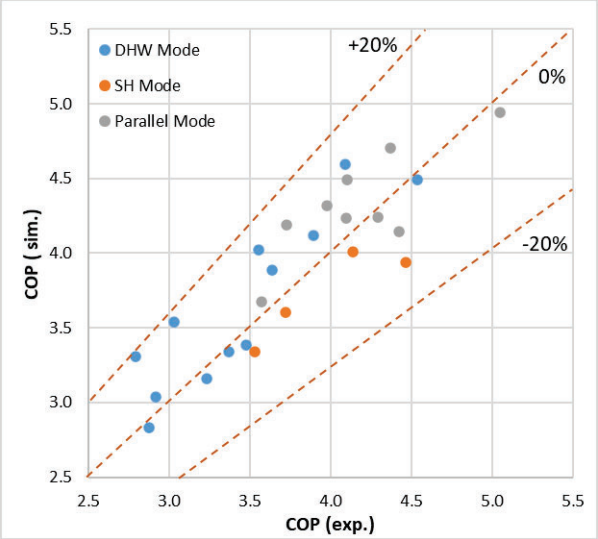

Figure 2: Validation results for the simulations under 25 different operating conditions.

3.2. Influence of Frequency and Heat Sink Temperatures on COP

The studied parameters of the presented simulation cases are mainly based on the prospective design values of the experimental heat pump. The COP investigation includes compressor frequencies from 25 Hz to 55 Hz. Additionally, DHW outlet temperatures from 55 °C to 70 °C are used for DHW and Parallel mode. For both modes, the DHW inlet temperature is set at 10 °C for all simulations. The SH mode is tested for three inlet/outlet temperature pairs, including 25/30 °C, 30/35 °C and 35/40 °C. The HP is fixed at constant values of 85 bar for the SH and Parallel mode and 105 bar for the DHW mode. Lastly, all simulations are carried out with an evaporator inlet/outlet temperature of 0/-3 °C. Figure 3 displays the effects on the COP for named conditions.

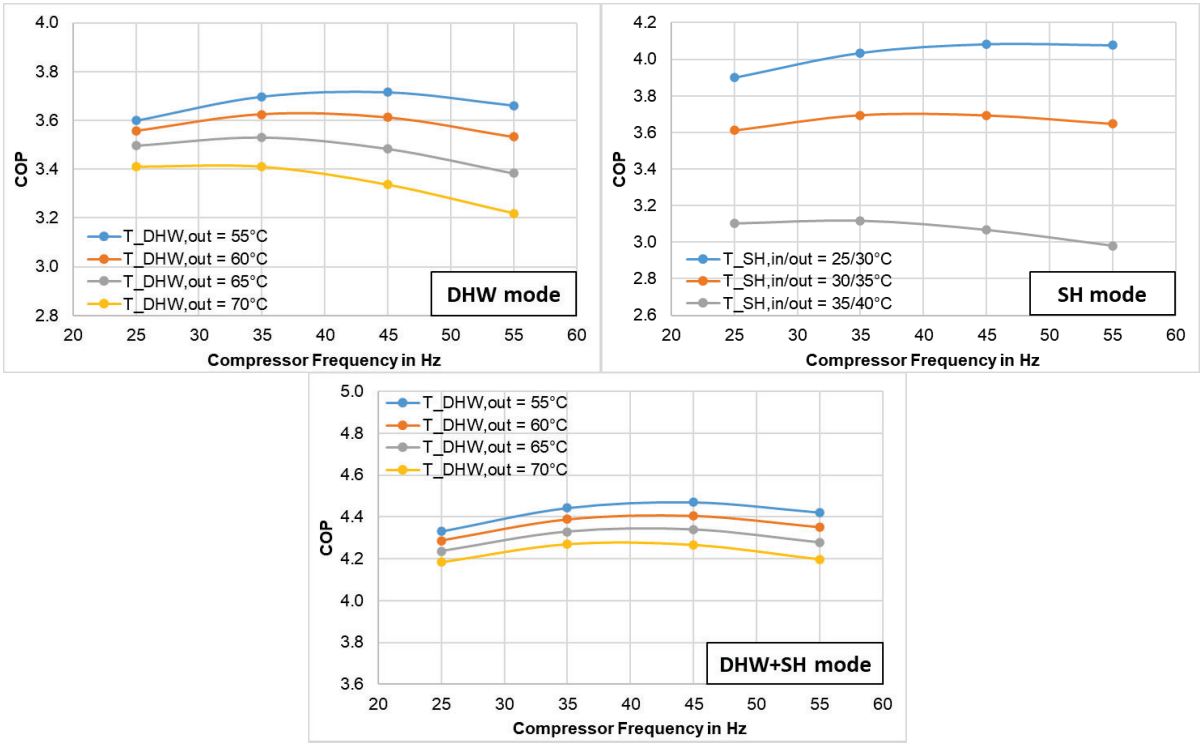

Figure 3: COP dependency with varying compressor speeds for different inlet/outlet temperatures for three heating modes.

The system COP decreases in all cases for an increase in DHW and SH temperatures. SH COP is especially sensitive to the temperature setpoint. In the case of 55 Hz and 35/40 °C the CO_2 leaves GC2 with 38.1 °C while at 25/30 °C it leaves with 28.4 °C. For higher SH temperatures the refrigerant is left with a larger quantity of residual energy, which consequently lowers system efficiency. Because of the lower GC3 DHW inlet temperature, the CO_2 energy has more utilization potential in DHW and Parallel mode. Despite of this, testing conditions with a high DHW outlet temperature also tend to affect the CO_2 outlet temperature adversely. For DHW mode, 55 Hz and a temperature rise from 55 °C to 70 °C, the CO_2 outlet temperature in GC3 also increases from 23.3 °C to 35.4 °C. To reach the higher DHW outlet temperature, it is observed that the DHW mass flow rate is reduced, inhibiting heat transfer in GC3. The largest difference between lowest and highest COP for the varied heat sink temperatures occurs in all cases at the maximum compressor frequency, with a COP loss of 15.0 %, 26.9 % and 4.5 % for DHW, SH and Parallel mode respectively. Parallel mode is therefore less sensitive to variations of the DHW outlet temperature. The decline in DHW mass flow rate, in consequence of higher DHW outlet temperatures, lead to higher GC2 inlet temperatures. This is followed by an increase of SH water mass flow rate to keep the SH temperature difference of 5 K. More heat is therefore supplied in GC2 which keeps the overall COP from declining. This circumstance is reflected in the behavior of the ratio between SH and DHW, which subsequently will be investigated in more detail.

3.3. Influence of Frequency and Heat Sink Temperatures on SH/DHW-Ratio

The SH/DHW-Ratio can be measured in Parallel mode, where DHW and SH are provided simultaneously. Just as the COP, the ratio between the SH and the DHW supply is subject to variation, if operating parameters are changed. Figure 4 shows the ratio for the Parallel mode simulation points displayed in Figure 3.

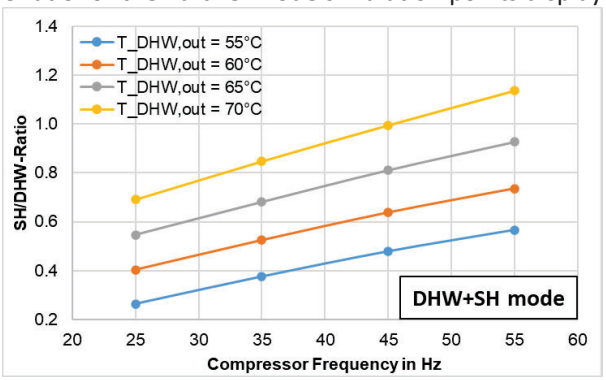

Figure 4: SH/DHW-Ratio with varying compressor speeds for different DHW outlet temperatures

Higher DHW outlet temperatures lead to higher SH/DHW-Ratios. This is explained by the temperature gradient between the water and the CO_2 and the corresponding change in water mass flow rate. With a rising DHW temperature setpoint, the difference between the CO_2 inlet temperature and the DHW outlet temperature gets smaller. At 55 Hz this temperature difference amounts to 35.3 K and 22.3 K for a DHW outlet temperature of 55 °C and 70 °C, respectively. In consequence, also the mean temperature difference between the refrigerant and the water in GC1 gets smaller. Equations (1) to (3) exemplary present the qualitative influence of this temperature difference on the DHW mass flow rate.

$$\dot{Q}_{CO2-DHW,GC1} = \overline{U} \cdot A_{GC1} \cdot \overline{\Delta T}_{CO2,DHW,GC1} \tag{1}$$

Equation (1) depicts the simplified stationary heat transmission in GC1 $\dot{Q}_{CO2-DHW,GC1}$ from the refrigerant to the DHW, where $\overline{U}$ presents the overall HTC, A_{GC1} is the total heat transfer area in GC1 and $\overline{\Delta T}_{CO2,DHW,GC1}$ is the mean temperature difference between the CO_2 and the DHW in GC1. Equation (1) can be equated with the specific heat formula on the DHW site $\dot{Q}_{DHW,GC1}$, which is presented in formula (2).

$$\dot{Q}_{CO2-DHW} = \dot{Q}_{DHW,GC1} = \dot{m}_{DHW} \cdot \bar{c}_{p,DHW,GC1} \cdot \Delta T_{DHW,GC1} \tag{2}$$

There, $\dot{m}_{DHW}$ displays the DHW mass flow rate, $\bar{c}_{p,DHW,GC1}$ is the mean isobaric specific heat of DHW in GC1 and $\Delta T_{DHW,GC1}$ presents the temperature difference between DHW outlet and inlet in GC1. It can now be rearranged for the investigation parameters. Since the overall HTC $\overline{U}$ is correlated with the DHW mass flow rate $\dot{m}_{DHW}$, it is included as a target parameter. Equation (3) shows the rearranged relation.

$$\frac{\dot{m}_{DHW}}{\overline{U}} = \frac{A_{GC1} \cdot \overline{\Delta T}_{CO2,DHW,GC1}}{\bar{c}_{p,DHW,GC1} \cdot \Delta T_{DHW,GC1}} \tag{3}$$

To show the proportional relation, the constants like the heat transfer area A_{GC1} and the near constant isobaric specific heat $\bar{c}_{p,DHW,GC1}$ are excluded. This yields equation (4).

$$\frac{\dot{m}_{DHW}}{\overline{U}} \sim \frac{\overline{\Delta T}_{CO2,DHW,GC1}}{\Delta T_{DHW,GC1}} \tag{4}$$

From 55 °C to 70 °C DHW outlet temperature, the mean temperature difference between the CO_2 and the DHW in GC1 declines, while the temperature difference between DHW outlet and inlet in GC1 rises. According to the relation in equation (4), the mass flow and the overall HTC declines. This is confirmed by the simulation results, yielding a reduction in DHW mass flow rate from 0.034 kg/s at 55 °C to 0.018 kg/s at 70 °C. This leads to less total heat supplied to the DHW, while more SH is provided. Furthermore, Figure 4 shows that rising frequencies also tend to raise the SH/DHW-Ratio. This is mainly evoked by the change in CO_2 mass flow and corresponding temperature changes. Since the ejector opening area is fixed by the set HP, a variation in compressor frequency leads to an almost equal change in CO_2 mass flow rate. For 55 °C DHW outlet temperature, raising the compressor frequency by 120 % (25 Hz to 55 Hz), leads to a raise in refrigerant mass flow rate of 137 % (0.0171 kg/s to 0.0403 kg/s). With an increase in mass flow rate of the refrigerant at higher frequencies, the temperature difference between inlet and outlet decreases in GC1. For 55 °C DHW outlet temperature and 25 Hz to 55 Hz, it decreases from 59.2 K to 49.1 K. With a lower temperature difference, the CO_2 leaves GC1 hotter, leading to a higher GC2 inlet temperature and a heat transfer advantage for SH. The results show that the lowest possible SH/DHW-Ratio is therefore reached if DHW outlet temperature and frequency are at their lowest possible values. To show the combined effects of frequency and DHW outlet temperature, Figure 5 compares the simulated cycles with the lowest and the highest SH/DHW-Ratio.

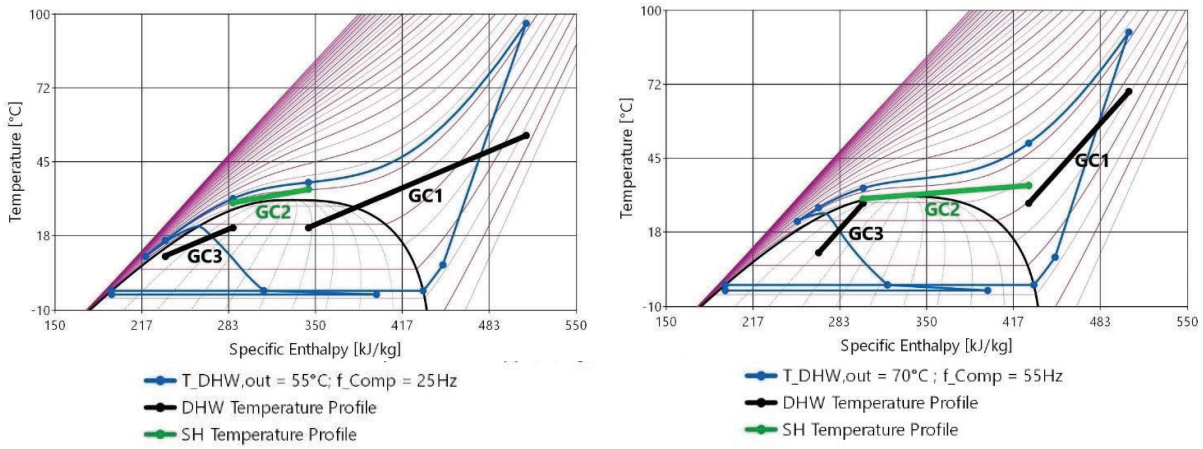

Figure 5: T-h-diagrams of the cycles with the lowest and the highest SH/DHW-Ratio with marked temperature profiles in the gas coolers.

For 25 Hz and 55 °C DHW outlet temperature, the ratio is 0.26, while at 55 Hz and 70 °C it amounts to 1.14. In the low-ratio case, the CO_2 enters GC1 with 96.7 °C, where the heat gets transmitted to DHW with a low mass flow rate and a setpoint of 55 °C. With this configuration the refrigerant gets cooled to a temperature of 37.5 °C before entering GC2. This suggests very advantageous heat exchange in GC1, approaching the setpoint of the SH temperature of 35 °C. Additionally, the lower mass flow rate in the DHW loop leads to more utilized energy for pre-heating in GC3. While for the 55 Hz and high CO_2 mass flow case it leaves GC3 with 26.7 °C, the temperature reaches as low as 16.0 °C in the 25 Hz and low mass flow rate case. A lower temperature means more energy is utilized in GC3, furthermore explaining the low SH/DHW-Ratio. Prospective investigations should encompass the impact of different SH temperatures, to get another degree of COP and SH/DHW-Ratio optimization options.

3.4. High Pressure Analysis for Optimal COP

The HP of the CO_2 has a crucial impact on how the heat rejection characteristic of CO_2 behaves. For each operating configuration an optimal HP value can be determined by which the COP reaches its maximum. The subsequent investigations will focus on the Parallel mode, where the best COP within a simulation condition is mainly determined by the combination of two heat transfer effects. While lower HP values benefit heat transfer properties of the CO_2 e.g., the isobaric specific heat capacity, higher HP more efficiently match the temperature profiles with higher temperature glides, especially considering DHW production. The maximum COP is reached at the point, where those two heat transfer effects are in their configuration-specific optimal relation. To find this optimum, the HP value for a set operating configuration is continuously lowered during a simulation from the starting value of 115 bar. The pressure is lowered until it reached 75 bar or the cycle collapsed. With the lowering of the pressure over a long period of time (t = 8000 s), a quasi-steady state is kept throughout the simulation. Subsequently, an analysis for the time at which the maximal COP occurred is done and result parameters are noted. One operating configuration per heating mode is tested. The evaporator inlet/outlet temperature is set at constant temperatures of 0/-3 °C. For the DHW and Parallel mode the DHW inlet/outlet temperature is set to 10/70 °C, while the SH inlet/outlet temperature is set to 30/35 °C for SH and Parallel mode. For every heating mode, seven different heat loads are investigated. They are mainly controlled by variation of the compressor frequency, regulating heat loads of up to 10 kW for DHW and Parallel mode and up to 8 kW for SH mode. The results are presented in Figure 6.

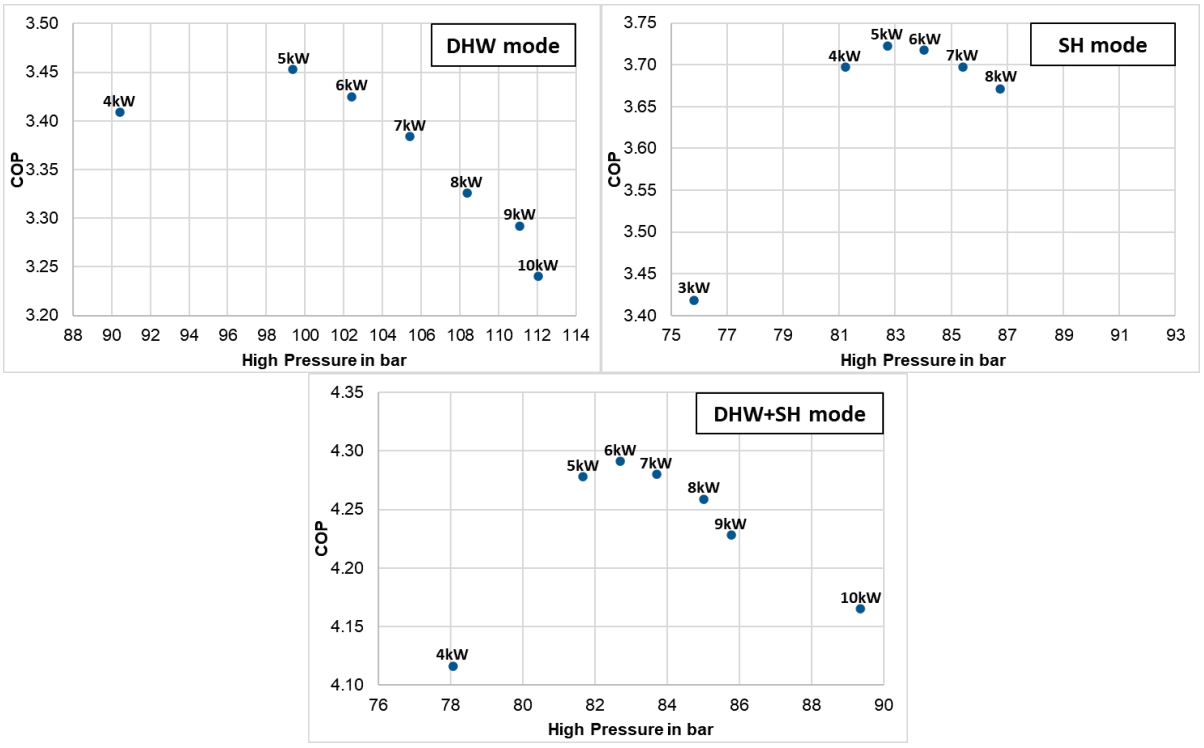

Figure 6: Highest simulated COP values in correlation to the high pressure at different heat loads.

The operation at 5 kW to 6 kW yields the best COP for the investigated operating conditions. The large pressure gaps, especially at the outer heat load points can be explained by the limits of the compressor frequency. In most of the cases, the frequency gets modulated in combination with the HP to reach the set heating capacity. If the compressor then reaches the limits of 25 Hz or 55 Hz, the capacity gets solely influenced by the HP modulation. Subsequently, a larger pressure step is necessary to reach the set value of the heat output. Outside the frequency limits of the compressor, the system COP gets influenced adversely. In DHW mode, the COP is lowered by 6.2 % by operating at 10 kW instead of 5 kW. While in DHW this effect is most pronounced between maximum load and partial load, SH and Parallel mode show similar behavior for low load, if compared to partial load. From 5 kW to 3 kW in SH mode and from 6 kW to 4 kW in Parallel mode, the COP falls by 8.2 % and 4.1 % for SH mode and Parallel mode, respectively. It is to mention that this

is dependent on the HP for a set heat source and heat sink temperature configuration. In this investigation, the HP could not be adjusted for inefficiencies when reaching compressor frequency limits, as the investigation encompassed the HP as the target parameter to optimize COP for a given heat load. Because for DHW mode a larger temperature glide is benefitting the efficiency, the optimum HP at 5 kW load is located around 100 bar. For SH and Parallel mode, this pressure is smaller as the SH temperature profile needs to be considered, which shows a better fit to the CO_2 temperature profile around 83 bar and partial loads. Pressures as low as 83 bar cannot be tested in the DHW mode, as they generally do not yield stable simulations in this mode. By simultaneously providing DHW and SH in Parallel mode, the COP maximum is improved by 24.3 % and 15.3 %, when compared to the maximum COP values of the DHW mode and SH mode, respectively.

3.5. SH/DHW-Ratio at Optimal COP

Lastly, the SH/DHW-Ratio in the Parallel mode for the seven different heat loads and at optimal HP will be analyzed. The results are taken from the simulations presented in Figure 6 and depicted in Figure 7.

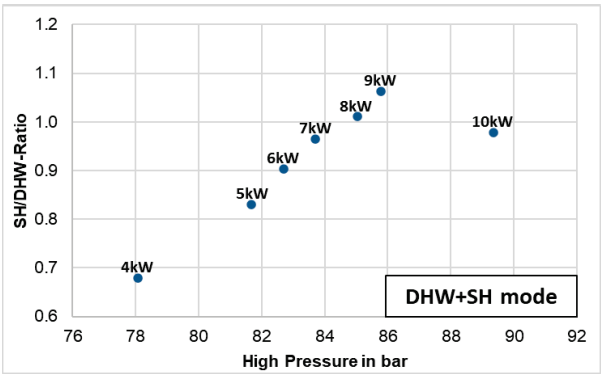

Figure 7: SH/DHW-Ratio at highest COP values in correlation to the HP at different heat output capacities.

The ratio behaves differently than the COP. While the COP has its maximum at 6 kW, the SH/DHW maximum is shifted to higher heat outputs. Just as with the COP investigations, the SH/DHW-Ratios get influenced by the compressor reaching its frequency limits. The heat load of 6 kW will therefore be compared to a heat load of 9 kW, which constitutes the highest possible load without distorting the comparison by reaching the compressor frequency limit. Both simulated cycles are shown in more detail in a p-h-diagram depicted in Figure 8.

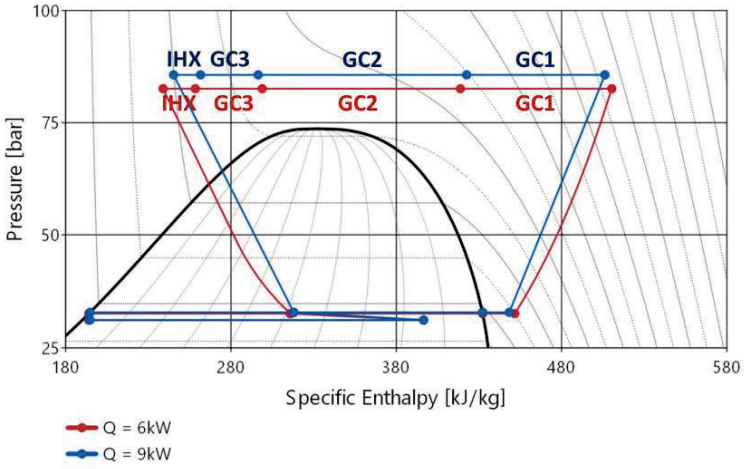

Figure 8: p-h-diagram of the cycles at 6 kW and 9 kW heat load, operated at a HP for optimal COP.

The comparison between both loads show that despite having a lower optimal HP at 6 kW, more DHW in proportion to SH is supplied. Hence, despite higher HP values generally benefitting DHW supply, they do not always lead to a smaller SH/DHW-Ratio. From 6 kW to 9 kW, the DHW heat output experiences a rise of 38.7 %, while the SH experiences a rise by 62.8 % in heat output, leading to a higher SH/DHW-Ratio at higher

HP. In accordance with the findings of chapter 3.3, this is caused by the increase in mass flow rate of the refrigerant. Corresponding to the increase of the compressor frequency from 35.3 Hz at 6 kW to 51.3 Hz at 9 kW, the CO_2 mass flow rate increases by 53.8 %. This leads to a smaller refrigerant temperature difference in GC1 and a higher GC2 inlet temperature, benefitting SH production. In conclusion, the SH/DHW-Ratio correlates highly with the mass flow rate of the CO_2, which defines how much heat is extracted in GC1 and how high the subsequent temperature level in GC2 is. For prospective investigations more temperature levels of the heat sinks should be regarded.

4. CONCLUSION

This study evaluates numerically the performance of a transcritical CO_2 heat pump with a novel brazed plate tri-partite gas cooler. After validating the model with experimental results, three modes are tested to expand investigation cases for the system. Different heat sink temperatures and their influence on the COP and SH/DHW-Ratio are investigated. The results show that at fixed heat source temperatures, high-pressures and DHW inlet temperatures, higher heat sink outlet temperatures lead to a lower COP. To achieve higher DHW temperatures the SH/DHW-Ratio rises as DHW mass flow rate declines. The same trend is observed with the rise of the compressor frequency and the higher corresponding CO_2 mass flow rates, as CO_2 leaves GC1 with a higher temperature level, benefitting SH supply in GC2. Furthermore, an approach for numerically analyzing an optimal HP is presented, where the COP can be analyzed for its highest value within a specified temperature configuration. The investigation is expanded for a range of heat loads. For all the investigated loads, partial heat load from 50 % to 60 % showed the highest COP. Parallel mode yields considerable higher COP compared to single modes, leading to improvements at optimal HP of up to 24.3 % and 15.3 % when compared to DHW and SH, respectively. SH/DHW-Ratio behaves independently from the COP, making it possible to find operating parameters that optimize both aspects simultaneously for a given heat demand.

ACKNOWLEDGEMENTS

This research is supported by the European Union's Horizon 2020 research and innovation program, 'TRI-HP project' (grant number 814888).

REFERENCES

[1] International Energy Agency, Ed., "Energy Technology Perspectives 2020: Flagship Report," Paris, Sep. 2020. [Online]. Available: https://www.iea.org/reports/energy-technology-perspectives-2020

[2] E. Brodal and S. Jackson, "A comparative study of CO2 heat pump performance for combined space and hot water heating," International Journal of Refrigeration, vol. 108, pp. 234–245, 2019, doi: 10.1016/j.ijrefrig.2019.08.019.

[3] F. Zhang, Y. Zhu, C. Li, and P. Jiang, "Thermodynamic optimization of heat transfer process in thermal systems using CO2 as the working fluid based on temperature glide matching," Energy, vol. 151, pp. 376–386, 2018, doi: 10.1016/j.energy.2018.03.009.

[4] S. Minetto, "Theoretical and experimental analysis of a CO2 heat pump for domestic hot water," International Journal of Refrigeration, vol. 34, no. 3, pp. 742–751, 2011, doi: 10.1016/j.ijrefrig.2010.12.018.

[5] Y. Zhu, Y. Huang, C. Li, F. Zhang, and P.-X. Jiang, "Experimental investigation on the performance of transcritical CO2 ejector–expansion heat pump water heater system," Energy Conversion and Management, vol. 167, pp. 147–155, 2018, doi: 10.1016/j.enconman.2018.04.081.

[6] Á. Á. Pardiñas, A. Hafner, and K. Banasiak, "Novel integrated CO2 vapour compression racks for supermarkets. Thermodynamic analysis of possible system configurations and influence of operational conditions," Applied Thermal Engineering, vol. 131, pp. 1008–1025, 2018, doi: 10.1016/j.applthermaleng.2017.12.015.

[7] J. Stene, "Residential CO2 heat pump system for combined space heating and hot water heating," International Journal of Refrigeration, vol. 28, no. 8, pp. 1259–1265, 2005, doi: 10.1016/j.ijrefrig.2005.07.006.

[8] Alireza Zendehboudi, Maike Schubert, Xabier Peña, & Raphael Gerber, “Critical review of heat pump prototype operation and required modications (V1.0): Deliverable number: D5.5,” TRI-HP, 2022. [Online]. Available: https://doi.org/10.5281/zenodo.5939491
[9] Association Modelica, Modelica. [Online]. Available: https://modelica.org/ (accessed: Jan. 25 2022).
[10] Dassault Systems, DYMOLA Systems Engineering. [Online]. Available: https://www.3ds.com/products-services/catia/products/dymola/ (accessed: Jan. 25 2022).
[11] TLK-Thermo GmbH, TIL Suite Thermal Systems: TLK-Thermo GmbH. [Online]. Available: https://www.tlk-thermo.com/index.php/en/til-suite (accessed: Jan. 25 2022).
[12] VDI Heat Atlas. Berlin, Heidelberg: Springer Berlin Heidelberg, 2010.
[13] John G. Collier, John R. Thome, Convective Boiling and Condensation, 3rd ed.: Clarendon Press, 1994.
[14] A. Zendehboudi, Z. Ye, A. Hafner, T. Andresen, and G. Skaugen, “Heat transfer and pressure drop of supercritical CO2 in brazed plate heat exchangers of the tri-partite gas cooler,” International Journal of Heat and Mass Transfer, vol. 178, p. 121641, 2021, doi: 10.1016/j.ijheatmasstransfer.2021.121641.

Open access to applied data:

Tom Ebel, Alireza Zendehboudi, Armin Hafner, & Dani C. Sanchez. (2022). Performance investigation of an ejector-assisted transcritical CO2 heat pump with brazed plate tri-partite gas cooler for space heating and hot water production [Data set]. Zenodo. https://doi.org/10.5281/zenodo.6538833